Intermetallics 18 (2010) 134–139

Contents lists available at ScienceDirect

Intermetallics

journal homepage: www.elsevier.com/locate/intermet

FeCo-based multiphase composites with high strength and large plastic deformation

R. Li [a,*], G. Liu [a], M. Stoica [a], J. Eckert [a,b]

[a] IFW Dresden, Institute for Complex Materials, P.O. Box 27 01 16, D-01171 Dresden, Germany
[b] TU Dresden, Institute of Materials Science, D-01062 Dresden, Germany

ARTICLE INFO

Article history:
Received 13 March 2009
Received in revised form
8 June 2009
Accepted 3 July 2009
Available online 21 July 2009

Keywords:
A. Composites
B. Mechanical properties at ambient temperature
B. Fracture mode
D. Microstructure
C. Rapid solidification processing

ABSTRACT

A family of FeCo-based multiphase composites with a microstructure consisting of nano-lamellar phase strengthened α-(Fe,Co) dendritic cores surrounded by a network of reinforcement phases of ultrafine eutectics was produced by copper mold casting. The hypoeutectic composites exhibit a high yield stress, which is up to 7 times higher than the equiatomic FeCo alloy, and plastic deformation up to 18% during compressive test. Multiscale *o*-$(Fe,Co)_3(B,C)$ reinforcement phases are responsible for the remarkable improvement of strength, and α-(Fe,Co) dendrites play a key role to inhibit the propagation of micro-cracks sourced from the eutectics. Furthermore, a fracture model for explaining the relationship between fracture strain and morphologic characteristics of the composites is presented.

1. Introduction

Recently, multicomponent metallic composites with high strength and large plastic deformation have been produced by copper mold casting in several hypoeutectic alloys [1–11]. These alloys display a characteristic microstructure consisting of soft dendritic cores surrounded by a hard network of ultrafine eutectics or metallic glasses (MGs). For example, composites consisting of β-Ti(Ta,Sn) dendrites embedded into a nano-eutectic matrix have been produced in multicomponent Ti-based alloys showing high yield strength of ~1.5 GPa, high compressive strength of ~2 GPa and large plasticity up to 10% under compressive conditions [1]. Materials with a similar dendritic-eutectic composite structure and remarkable mechanical properties (0.8–1.8 GPa yield strength, ~3.5 GPa compressive strength and ~10% plasticity) have also been produced in Fe-based alloys [7–9]. Under tensile conditions Zr- and Ti-based dendrite–MG composites show tensile strength of 1–1.5 GPa and ductility of 3–10% [3–6]. This kind of composite materials are promising candidates as advanced engineering materials due to the positive combination of the high strength typical of ultrafine-crystalline eutectic alloys or bulk metallic glasses with the plastic deformation of conventional crystalline materials. The deformation mechanism of this type of composites has been investigated in detail [1,4,7,9]. The high strength of the composites is attributed to the supporting framework of hard network phases combining with deformable dendritic phases suppressing the propagation of microcracks or shear bands. However, little attention has been paid so far to the quantitative relationship between mechanical properties and characteristic microstructure of this kind of composites.

The near-equiatomic FeCo alloy is a well-known magnetic material with high saturation magnetization and high Curie temperature, which is ideally suitable for the applications of high magnetic flux density in electromagnetic system [12,13]. Although independent multi-slips can occur during the plastic deformation of soft FeCo grains, this alloy is brittle at room temperature, therefore, limiting its industrial application. The brittleness of this alloy is a result of the intergranular fracture, which indicates the intrinsic weakness of the grain boundaries [13]. In this paper, a family of FeCo-based multiscale–multiphase composite alloys which overcome the brittleness of FeCo alloy has been produced by combining the relatively high cooling rate of copper mold casting with the appropriate design of the hypoeutectic multicomponent alloys. This results in the remarkable enhancement of the yield and fracture strength of the resulting alloys. Furthermore, the correlation between the mechanical properties and the microstructure (i.e., volume fraction and size of the multiscale phases) was successfully

* Corresponding author. Tel.: +49 351 4659 645; fax: +49 351 4659 452.
E-mail address: r.li@ifw-dresden.de (R. Li).

0966-9795/$ – see front matter © 2009 Elsevier Ltd. All rights reserved.
doi:10.1016/j.intermet.2009.07.003

evaluated via modeling, which gives a useful guideline to further develop this kind of composites.

2. Experimental procedure

Master alloys with nominal compositions $(Fe_{0.5}Co_{0.5})_x$-$(Mo_{0.1}C_{0.2}B_{0.5}Si_{0.2})_{100-x}$ ($x = 95$, 90 and 85) were prepared by melting the mixtures of pure elements in a induction furnace under an argon atmosphere. The three compositions are referred in this paper as FC95 ($x = 95$), FC90 ($x = 90$) and FC85 ($x = 85$). Rod-shaped specimens of 3 mm diameters and 50 mm length were produced using injection casting into a water-cooled copper mold. Phase structures were examined using a Philips PW 1050 X-ray diffractometer (XRD) with Co Kα radiation. The microstructure of the as-cast and the deformed samples was examined by scanning electronic microscopy (SEM) using a Gemini LEO 1530 microscope equipped with a Bruker energy dispersive X-ray spectrometer (EDX). The observed surface was etched in 5 vol% nitric acid–ethanol mixture for 10–25 s. Characteristic grain sizes and phase volume fractions were measured by image analysis. Hysteresis loops were measured with a Quantum Design PPMS® with a vibrating sample magnetometer (VSM) at ambient temperature in a DC magnetic field up to 25 kOe. Cylindrical samples with 3 mm diameter and 6 mm length were tested at constant strain rate ($1 \times 10^{-4}\ s^{-1}$) using an Instron 5869 testing facility. A laser extensometer (Fiedler) monitored the strain directly at the sample. At least five samples for each composition were tested under the same compressive condition to insure the reliability of the results.

3. Results and discussion

Fig. 1(a) shows the XRD patterns for three composites. The structure consists of a body centred cubic α-(Fe,Co) (bcc) solid solution together with a complex metastable Fe_3C-type *o*-$(Fe,Co)_3(B,C)$ intermetallic phase (space group: *Pnma*). The relative intensity of the diffraction peaks belonging to the $(Fe,Co)_3(B,C)$ phase increases with decreasing the FeCo content from $x = 95$ to $x = 85$, indicating a larger volume fraction of the $(Fe,Co)_3(B,C)$ phase in the corresponding alloys. According to EDX results, the ratio of Fe and Co contents in the α-(Fe,Co) and $(Fe,Co)_3(B,C)$ phases is found to be near 1:1 for all the composites. In contrast to former reports on multi-component Fe-based composites [7,9], no austenitic or martensitic phases have been observed in the present samples. A possible reason for this might be the enrichment of Si in the α-(Fe,Co) solution, which may favor the formation of the α-(Fe,Co) phase. Because of the high volume fraction of α-FeCo, these composites display a high saturation magnetization (B_s) (see Table 1). For example, the B_s for the FC95 composite (2.10 T) is as high as the value for pure iron.

SEM and EDX investigations reveal that the composites exhibit a uniform network structure with similar morphology and spatial distribution of the α-(Fe,Co) and $(Fe,Co)_3(B,C)$ phases. Fig. 1(b) gives a schematic illustration of the microstructural characteristics of the multiphase composites. As typical examples, SEM images of the FC90 sample are shown at low and high magnification (Fig. 1(c) and (d), respectively). The α-(Fe,Co) dendritic cores are surrounded by a network-like eutectic structure, consisting of α-(Fe,Co) and $(Fe,Co)_3(B,C)$, to form the dendrites–eutectics composite structure. Interestingly, a nano-lamellar $(Fe,Co)_3(B,C)$ phase of ~65 nm width

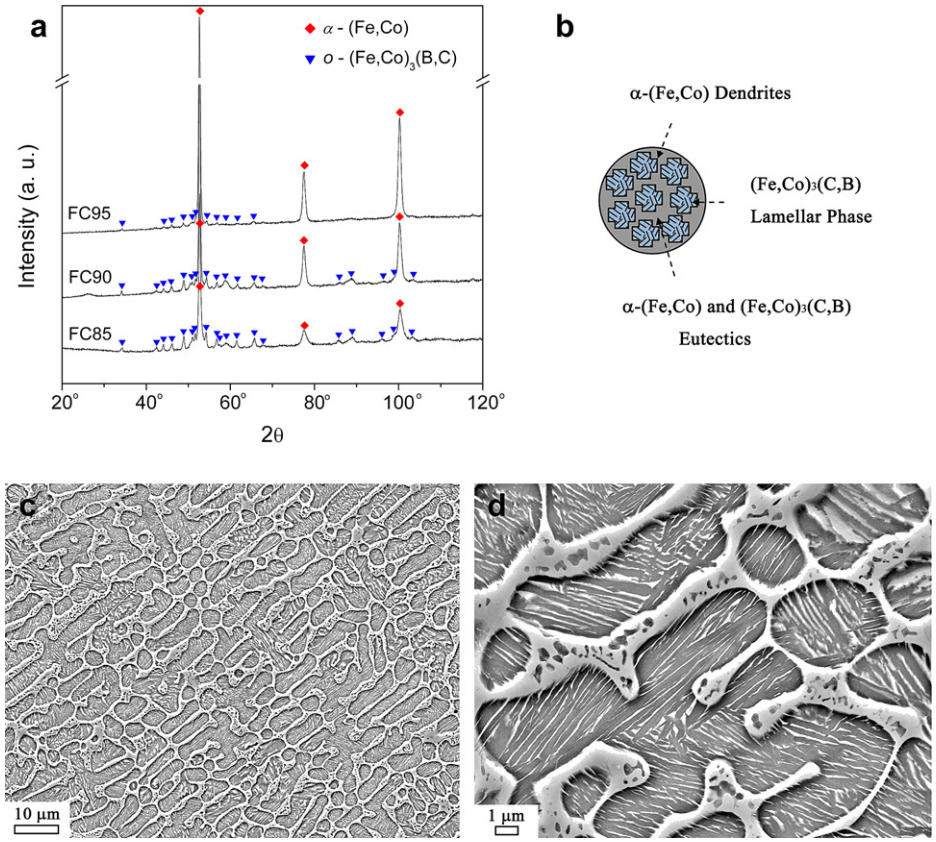

Fig. 1. (a) XRD patterns of the as-cast FC95, FC90 and FC85 composites. (b) A schematic illustration of the microstructural characteristics for the multiscale–multiphase composites. Typical SEM secondary electron images of etched cross-section for the FC90 at low magnification 1000 × (c) and high magnification 5000 × (d).

Table 1
Mechanical and material properties of FeCo-based multiscale–multiphase composites. The properties listed are yield strength (σ_y), yield strain (ε_y), compressive strength (σ_c), fracture strain (ε_f), modulus of elasticity (E), volume fraction of dendritic phase (f_d), mean linear size of dendritic phase (l_d), mean linear size of eutectic phases (l_e), strain hardening exponent (n), density (ρ), and saturation magnetization (B_s).

Name	Alloy	σ_y (MPa)	ε_y (%)	σ_c (MPa)	ε_f (%)	E (GPa)	f_d (%)	l_d (μm)	l_e (μm)	n	ρ (g/cm^3)	B_s (T)
FC95	$(Fe_{0.5}Co_{0.5})_{95}(Mo_{0.1}C_{0.2}B_{0.5}Si_{0.2})_5$	1153 ± 31	0.85 ± 0.01	2163 ± 76	18.62 ± 0.73	182 ± 7	79.8	6.1 ± 3.7	0.95 ± 0.83	0.17	8.087	2.10
FC90	$(Fe_{0.5}Co_{0.5})_{90}(Mo_{0.1}C_{0.2}B_{0.5}Si_{0.2})_{10}$	1514 ± 81	0.98 ± 0.10	2513 ± 38	6.05 ± 1.00	197 ± 18	63.5	3.1 ± 1.3	1.3 ± 1.1	0.26	7.984	1.87
FC85	$(Fe_{0.5}Co_{0.5})_{85}(Mo_{0.1}C_{0.2}B_{0.5}Si_{0.2})_{15}$	1936 ± 72	1.13 ± 0.12	2846 ± 86	2.75 ± 0.27	211 ± 13	49.3	2.2 ± 1.1	1.8 ± 1.3	0.30	7.894	1.74

and homogenously distributed in the α-(Fe,Co) dendrites is visible, leading to the formation of a secondary composite structure within the dendrites. The microstructure of similar soft dendrites–hard eutectics/MGs composites has been discussed for many alloy systems [1,4,7,10,11]. An appropriate volume fraction and average size of the soft and hard phases in the composite are expected to lead to good mechanical properties [5,6].

Quantitative microscopy was employed to evaluate the volume fractions and the average sizes of the constituent phases in the three composites by SEM image analysis [14]. (For every sample, at least five SEM images were analyzed.) The volume fraction of the dendritic phase (f_d), mean linear size of the dendritic phase (l_d) and mean linear size of the eutectic phases (l_e) are listed in Table 1. The value of f_d decreases from 79.8 to 49.3% with decreasing FeCo content (x) from 95 to 85. We find that f_d (or the volume fraction of the eutectic phases $f_e = 1 - f_d$) is approximately linearly dependent on x. These results indicate that the volume fractions of the constituent phases can be controlled by adjusting the composition of the hypoeutectic alloys. The value of l_d rapidly decrease with reducing x, while the dependence of l_d on x is opposite.

The stress–strain curves for the three composites are shown in Fig. 2(a) and the resulting mechanical properties are summarized in Table 1. The FC85 has the highest yield strength ($\sigma_y = 1936 \pm 72$ MPa) and compressive strength (the maximum strength) $\sigma_c = 2846 \pm 86$ MPa, while the FC95 exhibits the largest plastic strain $\varepsilon_p = \varepsilon_f - \varepsilon_y = 17.80 \pm 0.70\%$, where ε_y and ε_f are the strain at yield and the fracture strain, respectively. The strength (deformation capability) increases (decreases) in the sequence FC95 → FC90 → FC85. This indicates that the mechanical properties of such FeCo-based composites can be tuned by the proper choice of the chemical composition. The present composites with high FeCo content exhibit high values of σ_y that are 3–7 times higher than the equiatomic brittle precursor FeCo which shows low values of σ_y of about 300 MPa [12]. In addition, the multicomponent FeCo-based alloys display up to 18% plastic deformation, therefore, overcoming the weakness of the grain boundaries characterizing the binary FeCo alloys.

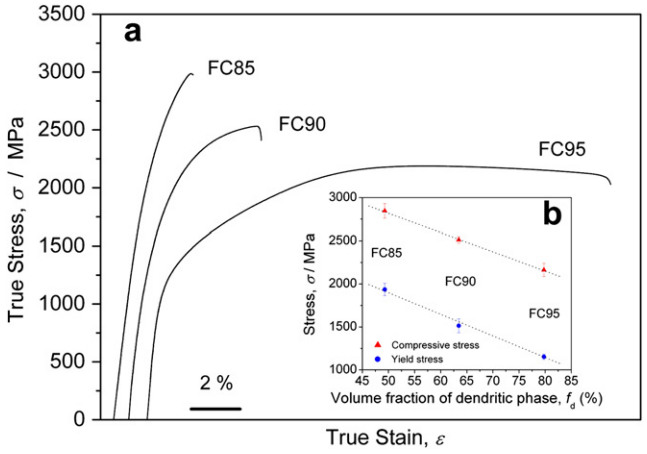

Fig. 2. (a) Typical compressive stress–strain curves for the as-cast FC95, FC90 and FC85 composites at room temperature. (b) Yield stress and compressive stress dependence on volume fraction of dendritic phase for the three alloys.

It has been reported that eutectic alloys produced by rapid solidification from the liquid can exhibit a superhigh strength, comparable to the value of bulk metallic glass, and a certain amount of plastic deformation [15,16]. The increase of volume fraction of the eutectic phases (f_e) with the decrease of x is most likely responsible for the improvement in strength and for the decrease of the deformation capability for the composites. With the assumption that the stresses in the two constituent phases dendrites and eutectics (σ_d and σ_e) are uniform, the stress (σ) of the FeCo-based composite can be given by the linear rule of mixtures [17]:

$$\sigma = f_d\sigma_d + f_e\sigma_e = \sigma_e + (\sigma_d - \sigma_e) f_d. \quad (1)$$

Eq. (1) indicates that the stress of composites is linearly dependent on the volume fractions of the constituent phases. This is in good agreement with the experimental measurements, as shown in the inset in Fig. 2(b), where both σ_y and σ_c show a linear relationship with f_d. By extrapolating $f_d \to 1$ (i.e., $f_e \to 0$), the yield strength of the FeCo dendrites (σ_y^d) was estimated to be about 640 MPa. The FeCo phase in the present alloys has a much larger yield strength than that of the traditional equiatomic FeCo alloy (300 MPa [12]). This is probably due to the strengthening effect of the nano-scale lamellar phase distributed within the FeCo dendritic phase (Fig. 1(d)). The results indicate that comparing with the equiatomic FeCo alloy the strength improvement in present composites is contributed by multiscale reinforcements, i.e., not only by micrometer scale eutectic phases but also by nano-scale lamellar phase.

The strain hardening exponent ($n = (\varepsilon/\sigma)(d\sigma/d\varepsilon)$) is an important parameter used to characterize the deformation behavior [18]. A high n value is usually related to the storage and interaction of dislocations in deformed materials [19]. In the present experiment, the values of n are 0.30, 0.26 and 0.17 for the FC85, FC90, and FC95 alloys, respectively. This indicates that n is also composition dependent or microstructure dependent. As discussed later, the deformation capability of the composites is related to n.

The cross-section of fractured samples was investigated by SEM to reveal the fracture mechanism of the composites. As a typical example, Fig. 3(a) shows the fracture surface of the FC90 alloys. The fracture process of the current FeCo-based composites can be described as follows: under the applied compressive strain/stress, microcracks appear in the relatively brittle eutectic phases (indicated by red arrows[1] in Fig. 3(a)) when local strain of the brittle phase is near to the deformation limit. The applied stress drives the microcracks to propagate mainly along the direction of resolved maximum shear stress (τ_m). However, the propagation of microcracks is retarded/suppressed by the plastic deformation of the dendritic phase that serves as ligament between adjacent microcracks, as demonstrated by Fig. 3(a), where local slip bands within the dendritic ligament can be clearly observed. With further

[1] For interpretation of the references to colour in this text, the reader is referred to the web version of this article.

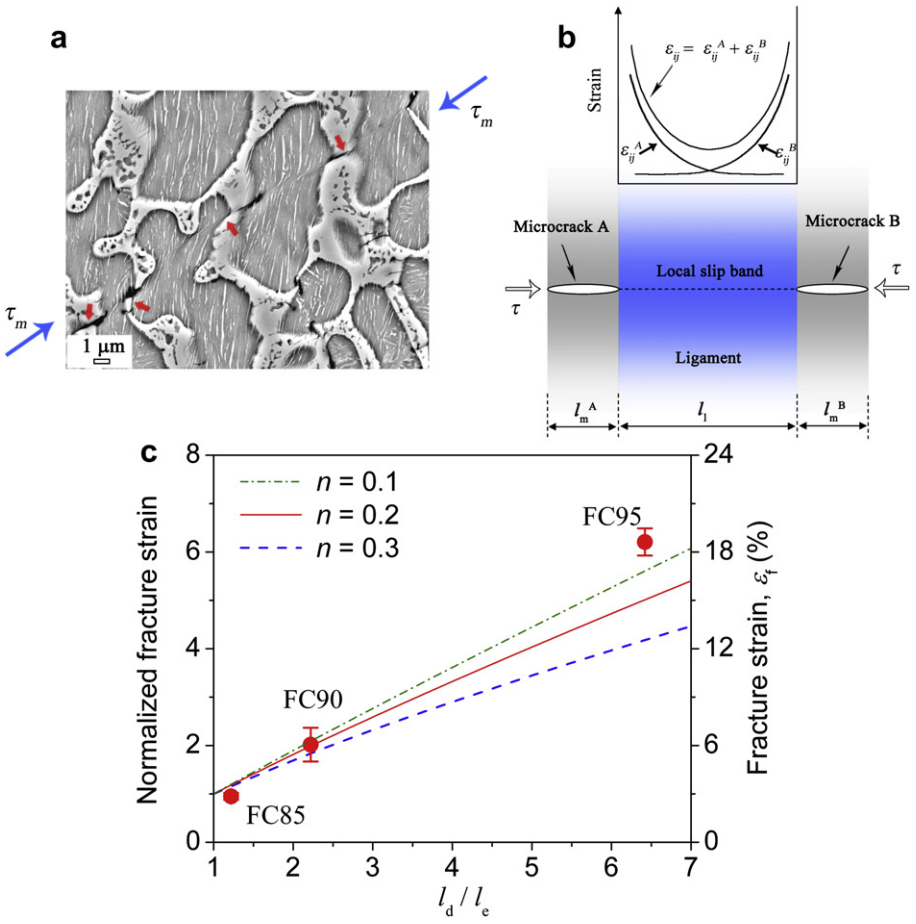

Fig. 3. (a) A typical SEM secondary electron image of etched cross-section for the fractured FC90 composite under compressive condition. τ_m is maximum shear stress. (b) A schematic illustration of the local fracture mechanism for the composites under shear stress (τ). (c) Dependence of normalized fracture strain/fracture strain on n values as a function of l_d/l_e for FC95, FC90 and FC85 composites.

increasing of the applied stress, the strain/stress fields ahead of the microcracks gradually rise, and the local plastic deformation within the dendrite phase is more and more intense up to a critical condition, where the ligament fracture leads to the failure of the whole specimen. This critical condition corresponds to the point of ε_f, which is believed to be sensitive to the microcrack size, the ligament size, and the plastic deformation capability of the dendritic phase [20,21].

There have been extensive works dedicated to study the influence of pre-formed microcracks or voids on the mechanical properties of metal materials, see for example [22,23]. Most recently, a micromechanical model [20,21] has been suggested to quantitatively describe the dependence of fracture strain on pre-formed microcracks, which has been successfully applied to Zr-based alloys [20] and Al-based alloys [21,24], both containing brittle second phase particles that are ready to fracture under applied stress. This model, based on fracture mechanics, is originally for Mode I fracture under applied tension stress and can be applicable to any metal based composites that contain brittle second phases or pre-formed microcracks. On the other hand, the stress fields ahead of crack tip in Mode II fracture (shear fracture) are similar to those in Mode I fracture, this model can be easily modified to be applicable for Mode II fracture. In present experimental, the brittle eutectic phases have been found to be ready to crack, forming pre-microcracks. The propagation and coalescence of pre-microcracks are mainly along the resolved maximum shear stress direction. This fracture process can be looked as a Mode II fracture. As a result, we can modify the aforementioned micromechanical model to relate ε_f to these influencing factors. In the model, the hard (eutectic phase) and the soft (dendritic phase) phases are assumed to be distributed alternatively (Fig. 3(b)). Under the applied stress, microcracks are pre-formed in the hard phase. These microcracks are initially stabilized by the soft phase. But the stress/strain fields ahead of the microcrack tip are intensified with increasing applied stress. In the ligament, the stress/strain fields of adjacent microcracks (microcracks A and B in Fig. 3(b), for example) are overlapped. Quantitatively, the strain tensor ε_{ij}^A ahead of microcrack A at a distance r is given from fracture mechanics as [25]

$$\varepsilon_{ij}^A = \alpha\varepsilon_y \left[\frac{J}{\alpha\varepsilon_y\sigma_y I_n r}\right]^{\frac{1}{1+n}} \tilde{\varepsilon}_{ij}(\theta), \tag{2}$$

where J is the J-integral, ε_y and σ_y are the yield strain and yield stress, respectively, $\tilde{\varepsilon}_{ij}(\theta)$ is a normalized parameter in the HRR field [25], n is the strain hardening exponent, I_n is a function of n

$$I_n = 10.3\sqrt{0.13+n} - 4.8n, \tag{3}$$

and α is the material constant in the Ramberg–Osgood constitutive relation

$$\frac{\varepsilon}{\varepsilon_y} = \alpha\left(\frac{\sigma}{\sigma_y}\right)^{1/n}, \tag{4}$$

with ε and σ being applied strain and stress. Similarly, the strain tensor at r due to microcrack B is given as

$$\varepsilon_{ij}^{B} = \alpha\varepsilon_y\left[\frac{J}{\alpha\varepsilon_y\sigma_y I_n(l_l - r)}\right]^{\frac{1}{1+n}}\tilde{\varepsilon}_{ij}(\theta), \quad (5)$$

where l_l is the width of ligament. Eq. (5) is added to Eq. (2) to yield

$$\varepsilon_{ij} = \varepsilon_{ij}^{A} + \varepsilon_{ij}^{B} = \alpha\varepsilon_y\left[\frac{QJ}{\alpha\varepsilon_y\sigma_y I_n r}\right]^{\frac{1}{1+n}}\tilde{\varepsilon}_{ij}(\theta), \quad (6)$$

where

$$Q = \left[1 + \left(\frac{r}{l_l - r}\right)^{\frac{1}{1+n}}\right]^{1+n}. \quad (7)$$

Eq. (6) represents the increase in the near-tip strains at r due to the interactions of microcracks A and B. One can easily obtained that the local strain tensor has the lowest value at $r = 1/2(l_l)$ or at the ligament center, as shown in Fig. 3 (b). The J-integral can be derived from fracture mechanics [25] as

$$J = \frac{0.405\pi h\sigma_y l_m(\varepsilon)^{1+n}}{(\alpha\varepsilon_y)^n}, \quad (8)$$

where l_m is the width of microcracks and h is a function of strain hardening exponent n [26]

$$h = \frac{3}{2\sqrt{1+3n}}. \quad (9)$$

Submitting above equation into Eq. (6) leads to

$$\varepsilon = \frac{1}{\tilde{\varepsilon}_n(\theta)}\left[\frac{I_n}{0.405\pi h}\right]^{\frac{1}{1+n}}\left[\frac{l_l}{l_m}\right]^{\frac{1}{1+n}}\frac{\tilde{\varepsilon}_r}{\left[1 + \left(\frac{r}{l_l - r}\right)^{\frac{1}{1+n}}\right]}, \quad (10)$$

where $\tilde{\varepsilon}_r$ is the local effective strain at r and $\tilde{\varepsilon}_n(\theta)$ is the effective value for the normalized coefficient $\tilde{\varepsilon}_{ij}(\theta)$. This equation relates the local effective strain at location r in the ligament to the nominal macroscopic strain ε. Fracture of the whole composites is taken to commence when the lowest local effective strain at ligament center ($r = (1/2)l_l$) reaches the fracture strain of the dendrite phase, ε_d, at $\theta = 0^\circ$ (shear fracture). The nominal fracture strain, ε_f, at the onset of fracture is then obtained from Eq. (10) by setting $\tilde{\varepsilon}_r = \varepsilon_d$, $\varepsilon = \varepsilon_f$, and $r = (1/2)l_l$ leading to

$$\varepsilon_f = \frac{1}{\tilde{\varepsilon}_n(0)}\left[\frac{I_n}{0.405\pi h}\right]^{\frac{1}{n+1}}\left[\frac{l_l}{l_m}\right]^{\frac{1}{n+1}}\frac{\varepsilon_d}{2}. \quad (11)$$

For calculation purpose in the present composites, the mean linear sizes of the dendritic and the eutectic phases, l_d and l_e, were taken as l_l and $l_{m,}$ respectively, to evaluate the fracture behavior of the dendrites–eutectic composite materials. ε_d is approximately a constant as for the FeCo dendrites phase. At this consideration, ε_f is a function of l_d/l_e and n. Calculations are performed using Eqs. (11), (9) and (3) to quantitatively reveal the dependence of ε_f on n as a function of l_d/l_e. The value of ε_d and $\tilde{\varepsilon}_n(0)$ is difficult to evaluate. However, these two parameters are constant. Normalization treatment can be then employed [24,27] in order to remove these constants. In present case, the fracture strain at $l_d/l_e = 1(\varepsilon_f^{l_d/l_e=1})$ is chosen as the reference and all the predicted ε_f will be normalized by $\varepsilon_f^{l_d/l_e=1}$. Following this treatment, calculated results of normalized fracture strain are shown in Fig. 3(c) to compare with the experimental results. The calculations are in good agreement with the experimental results. Eq. (11) clearly indicates that ε_f of the composites is related to the size of both constituent phases (l_d and l_e) and the deformation behavior of the ductile phase (n and ε_d). This model can be also applicable to other dendrites–eutectics/BGs composites with similar microstructures to achieve tunable mechanical properties by tailoring the microstructures, especially by artificially controlling the composition.

4. Conclusions

In summary, FeCo-based multiscale–multiphase composites, characteristic of nano-lamellar phase strengthened α-(Fe,Co) dendritic cores surrounded by network reinforcement phases of ultrafine eutectics in micrometer scale, were produced by rapid solidification. These composites exhibit 1.1–1.9 GPa yield stress and 2.2–2.8 GPa maximal stress as well as 3–18% deformation behavior during compressive test. A fracture model based on Model II is presented to reveal the relationship between fracture strain and morphologic construction of the constituent phases, which can be widely applied to evaluate and design this kind of composites.

Acknowledgement

The authors thank Dr. H. Wendrock for his valuable help on the SEM image analysis, and Dr. J.M. Park for helpful discussions. R. Li and G. Liu would like to acknowledge the fellowship support from the Alexander von Humboldt Foundation.

References

[1] He G, Eckert J, Loser W, Schultz L. Novel Ti-base nanostructure–dendrite composite with enhanced plasticity. Nat Mater 2003;2:33–7.
[2] Eckert J, He G, Das J, Loser W. Nanostructured composites in multicomponent alloy systems. Mater Trans 2003;44:1999–2006.
[3] Guo FQ, Poon SJ, Shiflet GJ. Networking amorphous phase reinforced titanium composites which show tensile plasticity. Philos Mag Lett 2008;88:615–22.
[4] Hofmann DC, Suh JY, Wiest A, Duan G, Lind ML, Demetriou MD, et al. Designing metallic glass matrix composites with high toughness and tensile ductility. Nature 2008;451:1085–93.
[5] Hays CC, Kim CP, Johnson WL. Microstructure controlled shear band pattern formation and enhanced plasticity of bulk metallic glasses containing in situ formed ductile phase dendrite dispersions. Phys Rev Lett 2000;84:2901–4.
[6] Hofmann DC, Suh JY, Wiest A, Lind ML, Demetriou MD, Johnson WL. Development of tough, low-density titanium-based bulk metallic glass matrix composites with tensile ductility. Proc Natl Acad Sci U S A 2008;105:20136–40.
[7] Kuhn U, Mattern N, Gemming T, Siegel U, Werniewicz K, Eckert J. Superior mechanical properties of FeCrMoVC. Appl Phys Lett 2007;90:261901.
[8] Park JM, Sohn SW, Kim DH, Kim KB, Kim WT, Eckert J. Propagation of shear bands and accommodation of shear strain in the $Fe_{56}Nb_4Al_{40}$ ultrafine eutectic–dendrite composite. Appl Phys Lett 2008;92:091910.
[9] Werniewicz K, Kuhn U, Mattern N, Bartusch B, Eckert J, Das J, et al. New Fe–Cr–Mo–Ga–C composites with high compressive strength and large plasticity. Acta Mater 2007;55:3513–20.
[10] Yavari AR, Ota K, Georgarakis K, LeMoulec A, Charlot F, Vaughan G, et al. Chill zone copper with the strength of stainless steel and tailorable color. Acta Mater 2008;56:1830–9.
[11] Lee ML, Li Y, Schuh CA. Effect of a controlled volume fraction of dendritic phases on tensile and compressive ductility in La-based metallic glass. Acta Mater 2004;52:4121–31.
[12] Sourmail T. Near equiatomic FeCo alloys: constitution, mechanical and magnetic properties. Prog Mater Sci 2005;50:816–80.
[13] Sundar RS, Deevi SC. Soft magnetic FeCo alloys: alloy development, processing, and properties. Int Mater Rev 2005;50:157–92.
[14] DeHoff RT, Rhines FN. Quantitative microscopy. New York, NY: McGraw-Hill; 1968.
[15] Das J, Kim KB, Baier F, Loser W, Eckert J. High-strength Ti-base ultrafine eutectic with enhanced ductility. Appl Phys Lett 2005;87:161907.
[16] Park JM, Kim DH, Kim KB, Kim WT. Deformation-induced rotational eutectic colonies containing length-scale heterogeneity in an ultrafine eutectic $Fe_{83}Ti_7Zr_6B_4$ alloy. Appl Phys Lett 2007;91:131907.
[17] Kainer KU. Metal matrix composites. Weinheim: Wiley-VCH Verlag GmbH & Co.; 2006.
[18] Llorca J, Needleman A, Suresh S. An analysis of the effect of matrix void growth on deformation and ductility in metal ceramic composite. Acta Metall Mater 1991;39:2317.
[19] Nabarro FRN. Theory of crystal dislocation. Oxford: Oxford University Press; 1967.

[20] Chan KS. A fracture model for hydride-induced embrittlement. Acta Metall Mater 1995;43:4325–35.
[21] Liu G, Zhang GJ, Ding XD, Sun J, Chen KH. The influence of multiscale second phase particles on ductility of aged aluminum alloys. Metall Mater Trans 2004;35A:1725.
[22] Van Stone RH, Cox TB, Low Jr JR, Psioda JA. Microstructural aspects of fracture by dimpled rupture. Int Met Rev 1985;30:157.
[23] Goods SH, Brown LM. Nucleation of cavities by plastic deformation – overview. Acta Metall 1979;27:1.
[24] Liu G, Zhang GJ, Wang RH, Hu W, Sun J, Chen KH. Heat-treatment-modulated coupling effect of multi-scale second phase particles on ductile fracture of aged aluminum alloys. Acta Mater 2007;55:273.
[25] Ewalds HL. Fracture mechanics. London: Edward Arnold; 1984.
[26] Dowling NE. *J*-Integral estimates for crack in infinite bodies. Eng Fract Mech 1987;26:333–48.
[27] Liu G, Sun J, Nan CW, Chen KH. Experiment and multiscale modeling of the coupled effect of constituents and precipitates on the ductile fracture of heat-treatable aluminum alloys. Acta Mater 2005;53:3459.